

**Origami magnetic cellulose: controlled magnetic fraction
and patterning of flexible bacterial cellulose**

Journal:	<i>Journal of Materials Chemistry C</i>
Manuscript ID:	TC-ART-04-2014-000787.R1
Article Type:	Paper
Date Submitted by the Author:	26-May-2014
Complete List of Authors:	Zeng, Mulling; Institut de Ciència de Materials de Barcelona (CSIC), Laromaine, Anna; Institut de Ciència de Materials de Barcelona, Feng, Wenqian; University of Heidelberg, Department of Applied Physical Chemistry; Karlsruhe Institute of Technology (KIT), Institute of Toxicology and Genetics (ITG) Levkin, Pavel; University of Heidelberg, Department of Applied Physical Chemistry; Karlsruhe Institute of Technology (KIT), Institute of Toxicology and Genetics (ITG) Roig, Anna; (ICMAB-CSIC), Institut de Ciència de Materials de Barcelona

Cite this: DOI: 10.1039/c0xx00000x

www.rsc.org/xxxxxx

ARTICLE TYPE

Origami magnetic cellulose: controlled magnetic fraction and patterning of flexible bacterial cellulose

Muling Zeng,^a Anna Laromaine,^{*a} Wenqian Feng,^b Pavel A. Levkin,^b Anna Roig^{*a}

Received (in XXX, XXX) Xth XXXXXXXXX 20XX, Accepted Xth XXXXXXXXX 20XX

DOI: 10.1039/b000000x

Cellulose of microbial origin is becoming a commodity structural material with promise in a myriad of potential applications. The range of applications can be further enlarged by nanocomposites that provide additional functional properties to the bacterial cellulose. Here, bacterial cellulose films nanocomposed with iron oxide nanoparticles are fabricated by microwave-assisted thermal decomposition within only 5 min and without need for any post-synthetic treatment. The in-situ synthesized nanoparticles are crystalline, less than 10 nm in size, and with a narrow particle-size distribution. Control over the magnetic fraction (from 4 to 40 %wt) is achieved either by employing undried cellulose, cellulose films dried by different methods, or by adjusting the initial iron precursor concentration. Structural, magnetic, and mechanical characterization of the materials is included. All films react easily to an external magnetic field, present a superparamagnetic behavior at room temperature, and are flexible enough to be bent and folded into complex origami shapes. Interestingly, films with low magnetic fraction are also transparent which is a highly attractive property for magnetic materials since most of them are either metallic or absorb visible light. Finally, preliminary results on a strategy to selectively pattern bacterial cellulose with nanoparticles are presented that pave the way to new uses of functional bacterial cellulose.

Introduction

Cellulose of microbial origin, commonly known as bacterial cellulose (BC), is becoming a commodity material since it incorporates desirable structural properties that are sought-after for the next generation of value-added materials.¹ A hierarchical porous network, high purity (absence of lignin and hemicelluloses usually present in cellulose from vegetal origin), high degree of polymerization and crystallinity (often larger than 70%) that leads to a high Young's modulus at room and elevated temperatures, extremely large water holding capacity (up to 100 times its own weight), and biological affinity make BC an important material for technological applications, including many in the healthcare sector.² For instance, due to its flexibility, strength, and conformability, films of BC can be used as wound-healing dressings in different contoured locations to prevent drying and infections in the healing site.³ Bacterial cellulose as a temporary skin is already patented and commercialized as BioFill®. In addition, BC can also be used in applications that require other functional properties; magnetic, electric, plasmonic, antimicrobial, among others. A possible strategy for use of BC in such applications is production of a nanocomposite of the BC with inorganic nanoparticles (NPs).⁴⁻¹¹ Nanocomposites of bacterial cellulose films with magnetic particles, which include different porous hierarchies as well as flexibility, could provide superior features compared to other traditional polymer matrices when used in several technological applications, such as: radio-frequency shielding materials^{4,12}, anti-counterfeiting papers¹³, ultra-thin loudspeakers¹⁴, flexible

data storage^{15,16}, heavy metal removal¹⁷ or biocompatible magnetic meshes for *in-vivo* uses to attract magnetized cells at target sites.¹⁸

Some of the challenges of this field are the achievement of sufficient and controllable NPs loading, not to compromise flexibility of the cellulose by the inorganic NPs load, NPs heterogeneous agglomerations or NPs leaching during the *in operando* conditions. An additional challenge is the development of economical and environmentally friendly methods to modify the surface of cellulose in large areas. We show here that microwave-assisted thermal decomposition is an efficient and fast method to attain uniform and controllable nanoparticles coating by using an inexpensive, green, scalable process. We have identified very few papers on the use of microwave heating for the synthesis of BC inorganic nanocomposites (calcium carbonate¹⁹ and silver nanoparticles).^{20,21}

Microwave heating represents an attractive non-conventional energy source for chemical synthesis due to the high acceleration and yield of the chemical reaction obtained.²²⁻²⁵ In comparison to conventional heating methods (heating plates, oil bath), microwave radiation avoids production of temperature gradients within the vessel, which decreases the possibility of asynchronic nucleation and heterogeneous nanocrystal growth. Microwaves heat polar substances rapidly and intensely, which makes possible to use them to heat selectively desired sites. In addition, microwave radiation induces molecular vibrations and a subsequent temperature increase that causes a greater movement of the molecules, high diffusivity and collision probability. Based on heating selectivity and the increase of the molecular motion,

complex nanostructured materials can be fabricated, such as in the case of conformal coating of porous materials by an *in situ* synthesis of a secondary phase.^{26,27}

Bacterial cellulose is formed by the polymerization of a glucose monomer, yielding a large number of surface accessible polar hydroxy groups that facilitate the chemical modification of BC, which permit modification of the hydrophilic character of the original BC or the incorporation of NPs into its structure.^{28,29} The hydroxy-terminated sites of BC scaffolds are more susceptible to absorption of microwave energy than the bulk of the material, and in this way the BC surface can be activated and the nucleation and the growth of the NPs on those sites promoted. Thus, hydroxy functional groups react with inorganic metal groups. The main interactions are driven by adsorption, van der Waals forces and electrostatic forces, as well as coordination/chelation linkages.²⁹ The ion-dipole interactions act as effective nanoreactor stabilizing the *in situ* as-prepared NPs via surface interactions.

Here, we report a one-step microwave-assisted chemical process that can grow a uniform conformal coating of superparamagnetic crystalline maghemite NPs on BC films within minutes. Previous magnetic bacterial cellulose nanocomposites were fabricated by using a multi-step *in situ* reduction of metal salts or dip-coating the cellulose into a NP suspension, which both offered poor control over the magnetic loading fraction.^{11,30} Here, by drying the cellulose films using different routes, we are able to tune the final amount of the magnetic content in the BC nanocomposites. The magnetic fraction can also be controlled, although to a lesser extent, by the initial iron precursor concentration. The method also allows a magnetic coating even of intricate figures shaped by origami. The magnetic cellulose is flexible and maintains the mechanical properties of the initial film. Finally, BC films are patterned with hydrophobic/hydrophilic domains and selectively anchor the magnetic NPs.

Experimental

Metals

Gluconacetobacter Xylinum (strain ATCC 11142) was purchased from CECT (Spain). Glucose, peptone, yeast extract, and agar were purchased from Conda Lab. NaOH, Na₂HPO₄·12H₂O, citric acid monohydrate, iron (III) acetylacetonate (Fe(acac)₃, 97%), benzyl alcohol, acetone, aqueous solution (25 wt %) of trimethylammonium hydroxide (TMAOH), and the reactants for the hydrophobization procedure were purchased from Sigma-Aldrich and were used as-received.

Production of bacterial cellulose films

Bacterial cellulose films were produced by *Gluconacetobacter Xylinum* (GX) in a conical flask at 25 °C. After 5 culture days, one big piece of BC film from the top of liquid media was harvested and boiled with deionized water (DI) and a 0.1 M NaOH solution to remove organic residues. After the alkali treatment, the BC film was immersed in DI water until neutralized. The clean BC film (labeled BC-wet) was cut into rectangular pieces (approx. 1 cm × 2 cm) and the pieces were dried by three different drying methods: room-temp drying, freeze-drying, and supercritical-drying, the samples were labeled BC-RD, BC-FD, and BC-SCD, respectively.³¹

Synthesis of magnetic cellulose films

Magnetic cellulose films were fabricated by *in situ* thermal decomposition of Fe(acac)₃ under microwave irradiation as follows: 0.35 mmol (123.6 mg) Fe(acac)₃ as iron precursor were dissolved in 4.5 mL benzyl alcohol.²⁵ BC-RD, BC-FD, BC-SCD, and BC-wet films were immersed in the solution for 30 min to ensure a homogeneous distribution of the precursor inside the cellulose network. Prior to that, the BC-wet film was subjected to a solvent exchange by immersing it in benzyl alcohol for 12 h.

Microwave (MW) experiments were carried out using a CEM Discover reactor (Explorer 12-Hybrid) operating at a frequency of 2.45 GHz and with a maximum power of 300 W. For a typical run, the power was automatically adjusted to heat the sample to the set reaction parameters (temperature and time). Temperature and pressure were monitored by using a volume-independent infrared sensor.

Solutions containing Fe(acac)₃ and the BC films were pre-heated to 60 °C for 5 min in the microwave reactor and further heated in the same reactor to 200 °C (typically using 300 W) for 5 min. Then, the solution was automatically cooled down to 50 °C using compressed nitrogen for approximately 3 min. Magnetic cellulose films were harvested from the solution and cleaned in a 10 mL acetone bath and sonicated for 3 min. NPs in suspension were separated by adding 40 mL acetone with 20 μL TMAOH (used as electrostatic surfactant) and centrifuged at 6000 rpm for 20 min. The supernatant from this first centrifugation was discarded; the precipitate was redispersed in the same amount of acetone with TMAOH and centrifuged again. The magnetic precipitate, after drying it overnight in an oven at 70 °C, was redispersed in 2 mL DI water containing 10 μL of TMAOH to yield a time-stable magnetic colloidal dispersion for further characterization.

In a second set of experiments, BC-RD films were treated using different Fe(acac)₃ concentrations: 0.156, 0.078, 0.039, and 0.02 M, labeled BC-RD-A, BC-RD-B, BC-RD-C, and BC-RD-D, respectively.

Hydrophobic patterning

Two rectangular pieces of BC-RD film (approx. 1 cm × 2 cm) were immersed in 25 mL of a dichloromethane solution containing 4-pentynoic acid (120 mg, 1.23 mmol) and 4-(dimethylamino)pyridine catalyst (56 mg, 0.46 mmol). The coupling reagent *N,N'*-diisopropylcarbodiimide (190 μL, 1.23 mmol), cooled to about 0 °C, was added to the solution, and the solution was stirred at room temperature for 4 h. The films were then washed extensively with ethanol, followed by drying. Next, the 4-pentynoic acid modified BC-RD film was placed on a glass substrate, wetted with acetone solution containing 10 vol% 1*H*,1*H*,2*H*,2*H*-perfluorodecanethiol, covered by a quartz slide, and irradiated with UV light (260 nm, 8.0 mw/cm²) through a quartz photomask for 60 s. After removing the photo mask, washing with acetone and drying, the film was wetted with 1:1 ethanol:water solution containing 15 wt% cysteamine hydrochloride and irradiated with UV light for another 60 s. Finally, the film was washed extensively with ethanol and dried gently with a nitrogen gun. After the first UV irradiation, the areas exposed to UV reacted with 1*H*,1*H*,2*H*,2*H*-perfluorodecanethiol to endow hydrophobicity. After the second

UV irradiation, the unexposed areas were functionalized with cysteamine hydrochloride to make them hydrophilic.

Characterization techniques

Thermogravimetric analysis (TGA): TGA of the magnetic cellulose films was performed with a TGA-DSC/DTA analyzer (NETZSCH STA 449 F1 Jupiter, ICMAB) with a heating rate of 10 °C/min from room temperature to 800 °C in air.

Scanning electron microscopy (SEM): Samples placed on an SEM aluminum substrate over a carbon-tape adhesive were imaged with a scanning electron microscope (QUANTA FEI 200 FEG-ESEM) under high-vacuum conditions, an acceleration voltage of 10-30 kV, an electron beam spot of 3.0, a pressure of 2 to 9×10^{-4} Pa, and a distance of 4 - 4.5 mm.

Transmission electron microscopy (TEM): TEM images were obtained with a JEOL JEM-1210 electron microscope, operating at 120 kV. The NPs' mean size was calculated by fitting a size histogram of the at least 200 nanoparticles to a Gaussian function. The standard deviation (σ) is defined as the root of the average of the squares of the differences of all the observations from their mean size, and the polydispersity of the distribution (P) is defined as the percentage of the standard deviation (σ) related to the mean size ($P = (\sigma / \text{mean value}) \times 100$)

Superconducting quantum interference device (SQUID): Magnetic characterization was performed with a superconductive quantum interference device (SQUID) magnetometer (Quantum Design MPMS5XL). The evaluation of the magnetic properties comprises the measurement of the magnetization *versus* the applied magnetic field at a constant temperature (M(H) curves at 300 K) and magnetization *versus* the temperature at a constant applied magnetic field (ZFC-FC curves at 50 Oe).

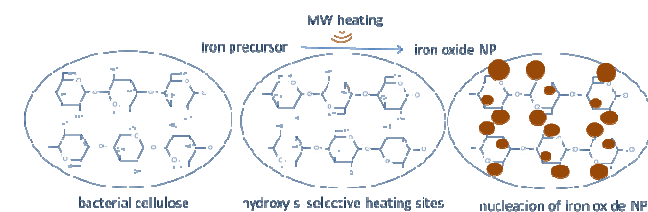
Mechanical properties: Hardness, Young's modulus and Elastic parameter (EP %) of magnetic BC films were obtained with a nanoindenter (Nanoindenter XP system) with a Berkovich diamond indentation tip. All samples were cut into 0.5 cm \times 1 cm pieces and were fixed flat on the holder using double-sided tape without any further preparation. Indentation curves were obtained at a loading and unloading rate of 0.08 mN/s and maximum load of 0.4 mN. Pristine and magnetic BC films were measured ten times in regions separated within 20 μ m per measurement to evaluate and average the whole surface. Elastic parameter (EP) was computed by using: EP % = (penetration depth at max loading - penetration depth after unloading)/(penetration at max loading) %.

Water absorption capacity (WAC): BC films before and after microwave reactions were dried and weighed. Films were immersed in DI water for 2 h. Excess water was removed and films were weighed once more. The WAC was calculated as $WAC = (w_{\text{wet}} - w_{\text{dry}}) / w_{\text{dry}}$, where w_{wet} is the weight of wet films and w_{dry} is the initial weight of the dry films.

Contact-angle measurement/drop-shape analysis system: Contact-angle measurements were performed with a Krüss DSA 100 Drop Shape Analysis System. Magnetic cellulose films were fixed flat on the top of a glass slide. A droplet of water (5 μ L) was placed on top of the BC films. The droplet was illuminated from the side and contact angles were calculated by using ImageJ analysis software.

Results and discussion

Bacterial cellulose harvested after five days from *Gluconacetobacter xylinum* culture was cut into rectangular pieces (ca. 2 \times 1 cm) and dried by using different procedures; room temperature solvent evaporation (BC-RD), freeze drying by sublimation of the frozen solvent (BC-FD), and supercritical CO₂ evacuation after solvent exchange to liquid CO₂ (BC-SCD). We also evaluated the never-dried film (BC-wet). In all cases, films were less than 200 μ m thick and extensively characterized in previous work.³¹ The films were immersed in microwave-oven flasks with a solution containing iron acetylacetonate, as the iron oxide precursor, in benzyl alcohol. Magnetic cellulose films were obtained after 5 min reaction at 200 °C. Scheme 1 contains the proposed mechanism of the procedure.⁶ The chemical reaction of iron oxide NPs starts with the formation of Fe(OH) monomers from the precursor of Fe(acac)₃ and benzyl alcohol, in similar way as reported by Bilecka et al.²³ for zinc oxide. In our case, the precursor is iron (III) acetylacetonate and the mechanism is an aldol condensation³² instead of an ester elimination reaction. Some theoretical models of mechanism in microwave have been proposed by S. Kalhori et al.³³



Scheme 1. Proposed mechanism of the bacterial cellulose-iron oxide nanocomposites.

A second set of experiments was completed under the same conditions by placing room-temperature cellulose films (BC-RD) in solutions containing decreasing concentrations of iron acetylacetonate (BC-RD-A,B,C,D). In both cases the magnetic fraction was calculated by TGA as well as by weighing the cellulose films before and after the synthesis of the magnetic nanoparticles; the results were coincident.

Figure 1 shows the pristine BC and the magnetic BC films. Films were not damaged during the microwave synthesis and present a macroscopic uniform coverage of the magnetic coating. Moreover, the series BC-RD-A,B,C,D also shows great transparency. The BC-RD-A film was slightly damaged during the cleaning step. All films readily responded to an externally applied permanent magnet. Figure S1 contains a video of the response of the BC-SCD sample to an external magnetic field.

Magnetic loading ranged from 4 %wt of the BC-RD-D material exposed to the lowest iron precursor concentration to up to 40 %wt for the never-dried cellulose, BC-wet, as determined by using TGA (Fig. S2). These values are depicted in Figure 2 where the concentrations of the NPs recovered from the supernatant after the reactions are also included. Figure 2 shows the great influence of the drying procedure used for the cellulose films in the magnetic loading of the final material. BC-wet and BC-SCD films allowed up to 40 % magnetic loading, while BC-RD could only reach 7 %. This result can be related to the porosity of the starting material (90 %, 80 % and 60 % for BC-SCD, BC-FD,

BC-RD, respectively) and thus to the number of accessible hydroxy groups.³¹

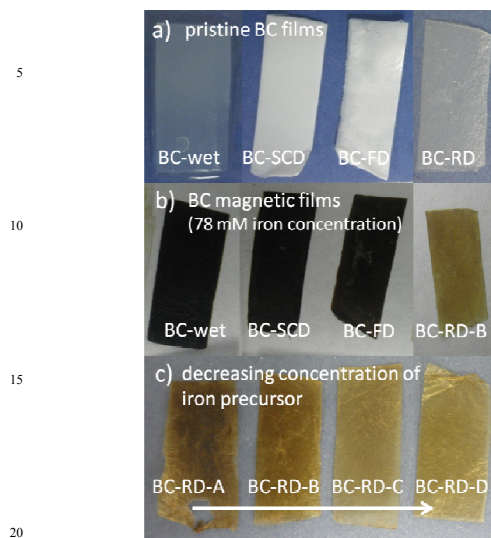


Fig. 1 (a) Digital images of the initial pristine BC-films without drying and dried by different routes. (b) Magnetic nanocomposite films synthesized using the same concentration (78 mM) of iron precursor. (c) Magnetic nanocomposite films produced from the BC films dried at room temperature (BC-RD) and using decreasing amounts of iron precursor concentration (160-20 mM).

The concentration of initial iron precursor can also be used to control the magnetic loading, although to a lesser extent than the drying method. An increase to eight times the initial concentration results in only 2.5-fold increase of the magnetic loading (from 4 % for 20 mmol/L to 9 % for 160 mmol/L). In all cases an excess of iron precursor ($\text{Fe}(\text{acac})_3$) was available, as can be seen by the resulting colloidal dispersions of the recovered NPs that were not attached to the cellulose. Therefore, we conclude that the amount of accessible hydroxy groups in the cellulose films is a determining factor in controlling the magnetic loading of the films.

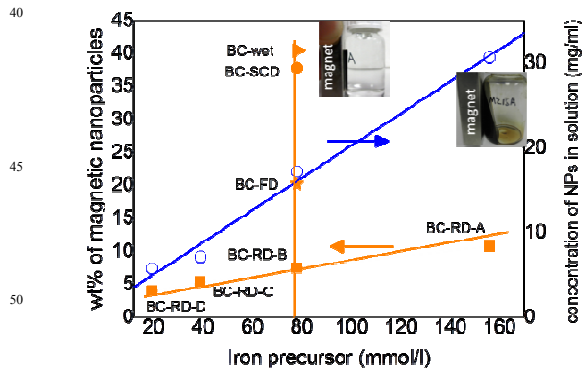


Fig. 2 Left y-axis represents the magnetic fraction of the magnetic films vs initial iron precursor concentration (full orange squares and orange line as a visual guide to show the linear dependence). Right y-axis represents the concentration of iron oxide nanoparticles in solution, recovered from the supernatant (empty symbols and blue line as a visual guide to show linear dependence). At 78 mM initial iron precursor concentration the magnetic fraction of the magnetic films is depicted for the several the drying routes used (full orange symbols, square, star, circle and triangle).

Images illustrating the attraction of BC-SCD film and nanoparticles in solution to a small permanent magnet are also included.

Figure 3 illustrates the hardness and flexibility of the magnetic films under applied pressure/weight, two key properties of our films. The first row of pictures shows some digital images of the BC magnetic films holding a solid wax droplet (approx 25mg), which indicate that the films do not break when weighted; the second row demonstrates the flexibility of the magnetic cellulose when it is rolled over, while the ability of the films to recover their original shape is shown in the third row. BC-RD-B is also transparent, which is clearly depicted in the figure inset.

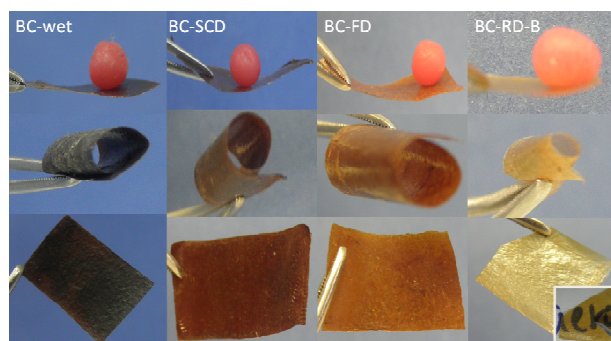


Fig. 3 Upper row: Images of the magnetic BC-films holding a wax ball. Middle row: Flexibility of the materials is illustrated by rolling them up. Lower row: Materials recovered their initial flat shape after being rolled. Inset: BC-RD-B film transparency is evidenced.

Figure 4 shows electronic microscopy images of magnetic cellulose films. A SEM image of BC-SCD allows us to identify the cellulose fibers and the NPs as well as the uniform conformal distribution of the NPs on cellulose fibers (Figure 4a). Figure 4b contains a TEM image of BC-RD-B; use of transmission mode was possible due to the film thickness (under 100 μm) and the relatively low magnetic load (7 %) of this sample. In this case, cellulose fibers are more clearly seen than during the SEM observation and the magnetic nanoparticles are individually distinguishable, which allows us to calculate the particle size histogram; this gives a mean size of 5.8 nm (inset of Figure 4b). The particles are placed over the cellulose fibers and not within the pores; this observation validates the hypothesis that the nanocrystals preferentially nucleate in the hydroxy groups of the cellulose. Figure 4c presents the TEM image of the NPs in solution and the inset contains a size histogram with the same mean size of 5.8 nm; the nanocrystals in solution and those attached to the cellulose have the same size. The electron diffraction patterns of selected areas (insets of Figs 4b and 4c) were used to identify the iron oxide phase and were indexed with the maghemite diffraction planes in both cases (see Fig. S3).

Figure S4 shows a series of images of the magnetic cellulose films immersed in water, in which the water remained completely uncolored even after two months, which thus points to the lack of nanoparticle leaching. Thermogravimetry of a BC-RD-B film was performed after 3 months to confirm the lack of NP leaching (shown in Fig. S2b).

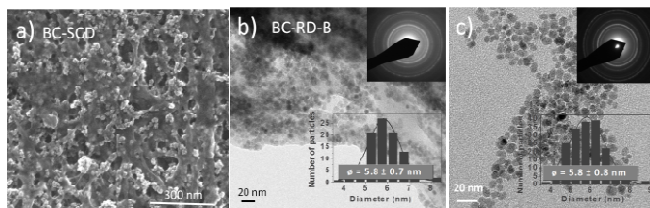


Fig. 4 (a) SEM image of the magnetic BC-SCD film; cellulose fibers can be distinguished from the NPs, homogeneity and conformal distribution of the magnetic load can be inferred. (b) TEM image of the BC-RD-B; cellulose fibers and individual NPs can be clearly observed here. (c) TEM image of NPs in solution. Upper insets of (b) and (c): Selected area electron diffraction patterns; lower insets: Particle size histograms and mean particle size values.

The magnetic properties of the nanocomposite cellulose for the RD series are summarized in Figure 5. Plots of magnetization *versus* field, $M(H)$ (Fig. 5a), and field-cooled/zero-field-cooled (FC-ZFC) (Fig. 5b) normalized to grams of iron oxide showed that all curves collapsed to a single one, which indicates identical magnetic behavior for the four samples despite their different magnetic loading fractions. The saturation magnetization value is approximately 30 $\text{emu/g Fe}_2\text{O}_3$; a rather modest value for crystalline maghemite particles of 6 nm diameter. The lack of remanence and coercivity evidence the superparamagnetic behavior of the films, which is also confirmed by the characteristic features of the FC-ZFC plots displayed in Figure 5b. Figure 5b also allows us to point out three more features. Firstly, all four samples exhibit the same maximum for the ZFC curves that signals the blocking temperature ($T_B \approx 50$ K), which thus indicates that the particle volume is the same in all the films. Secondly, the sharpness of the ZFC curves indicates that the particle assembly has a narrow particle size distribution, as already observed by the size histogram from the TEM images. Finally, the sharp increase of the FC curve at very low temperature could indicate a paramagnetic component in the system, which likely arises from Fe^{3+} ions bonded to the cellulose, and which in turn may explain the rather moderate value of the saturation magnetization values.

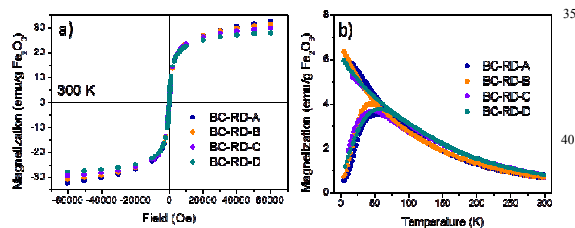


Fig. 5 (a) Magnetization ($\text{emu/g Fe}_2\text{O}_3$) *vs.* magnetic field at room temperature of the series of magnetic bacterial cellulose films with decreasing initial iron concentration. (b) Magnetization ($\text{emu/g Fe}_2\text{O}_3$) *vs.* temperature for the same series measured with a 50 Oe applied field.

Figure 6 includes the magnetic characterization for the sample with the largest magnetic fraction, BC-wet. Essentially the same magnetic behavior as that described above can be recognized here also. In this case the NPs' volume is slightly larger, as seen by the increase of the blocking temperature ($T_B \approx 100$ K; see inset of

Figure 6). The FC curve does not show a prominent increase at low temperature but rather levels off to a given value (16 $\text{emu/g Fe}_2\text{O}_3$), which indicates that no paramagnetic component is present in this sample. These two features lead to a larger magnetization saturation value (ca. 60 $\text{emu/g Fe}_2\text{O}_3$) for this system than for the previously described ones. Figure 6b includes a TEM image and size histogram of the NPs in suspension formed during the coating of BC-wet supporting a larger nanoparticle mean size (8.7 nm) compared to the previously discussed system (5.8 nm). TEM investigation of BC-wet film was not possible since the high magnetic load prevented electronic transmission through the film. Several repeats of this experiment were made and they confirmed the result that a large NP size was always found in BC-wet, however, at this point we do not have a plausible explanation for this fact.

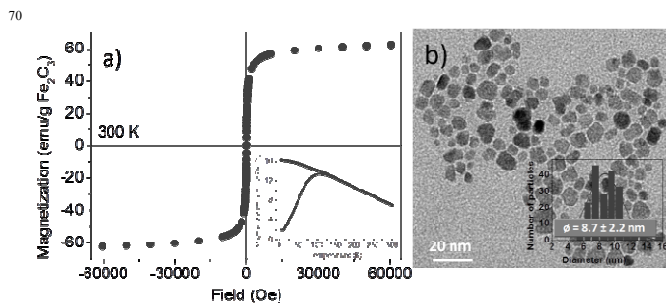


Fig. 6 (a) Magnetization ($\text{emu/g Fe}_2\text{O}_3$) *vs.* magnetic field at room temperature of magnetic BC-wet. Inset: Magnetization ($\text{emu/g Fe}_2\text{O}_3$) *vs.* temperature measured with a 50 Oe applied field. (b) TEM image of NPs in solution. Inset: Particle size histogram and mean particle size value.

Through mechanical characterization by nanoindentation, we find that the load-displacement curves obtained by nanoindentation of BC-RD and the nanocomposite one (BC-RD-B) exhibit similar elastoplastic behavior, which indicates that the nanoparticle coating does not affect the mechanical characteristics of the cellulose. Moreover, untreated BC is hydrophilic (contact angle almost zero) and has a very high water absorption capacity (WAC). Pristine BC-RD has a WAC of 34, which means that it can absorb and hold up to 34 times its own weight in water. Magnetic cellulose film BC-RD-B has a less hydrophilic character than the pristine one, which is likely associated with an increase of surface roughness provided by the NPs in BC-RD-B, while the WAC value diminishes to 7 from an initial value of 34 in the pristine film (inset of Fig. 7, Table S1 for the WAC and contact-angle values).

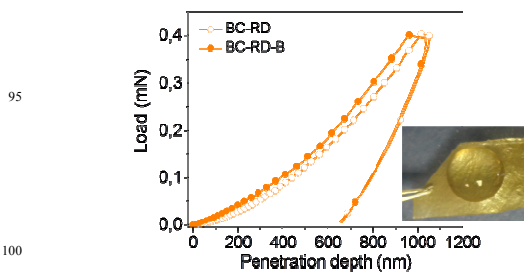


Fig. 7 Loading and unloading displacement curves of pristine BC film dried at room temperature (empty symbols) and magnetic BC-RD-B (full symbols). Inset: A droplet of water on BC-RD-B.

To further show the flexibility of the BC films we constructed a small origami swan with a square piece of paper $1.5\text{ cm} \times 1.5\text{ cm}$ (see Fig. 8). The bacterial cellulose swan was also conformally and uniformly coated with superparamagnetic nanoparticles, which demonstrates that our method allows the fabrication of intricate magnetic light objects. Thus, microwave synthesis at high temperature doesn't damage the cellulose fibers and selective nucleation on the hydroxy groups is extended to any part of such intricate shape. Figure S5 contains a video of the magnetic origami "dancing" under an applied magnetic field.

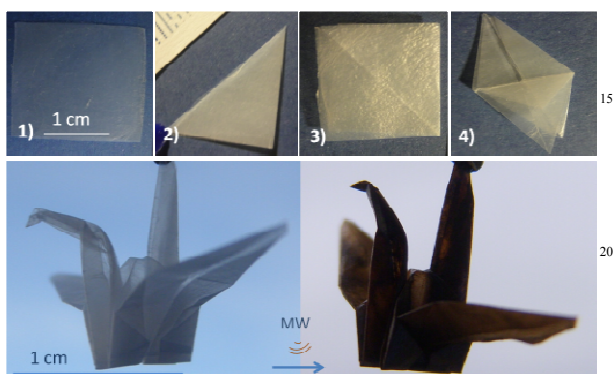


Fig. 8 Upper row: Folding steps to construct an origami swan out of bacterial cellulose. Lower row: Final result is depicted which also includes the "magnetic origami" after being treated in a microwave oven for 5 min with the iron precursor.

Finally we investigated the possibility of producing patterned BC by inducing selective nucleation of magnetic nanoparticles in the films. In this way we could obtain biodegradable magnetic micromeshes that, once magnetized, allow the creation of complex field patterns and attract magnetic nano-objects or magnetized cells to the spots with the highest field gradient. A demand for this type of material was clearly stated by Fu et al.,¹⁸ who used a highly toxic nickel mesh to enhance cancer targeting in living subjects and mentioned the need for biocompatible micromeshes for clinical implementation of the technology. We patterned pristine BC-RD samples with cysteamine (hydrophilic zones) and hydrophobic zones terminated by non-polar $1H,1H,2H,2H$ -perfluorodecanethiol. Patterns are shown in Figure 9. We hypothesized that the nucleation and growth of iron oxide nanoparticles will be mostly favored in the hydrophilic part of the BC film. Preliminary results showed that indeed the hydrophilic parts are darker, which indicates a larger fraction of NPs (50 % larger magnetic load in the hydrophilic zone than in the hydrophobic one, as measured by TGA; Fig. 9 and TGA in Fig. S2c). Further studies will be needed to optimize this approach since not all of the hydroxy groups reacted with 4-pentynoic acid in the esterification step and both hydrophobic and hydrophilic areas contained residual hydroxy groups, moreover, benzyl alcohol partially hydrolyzes the hydrophobic groups and thus some magnetic coating is also visible in the hydrophobic part.

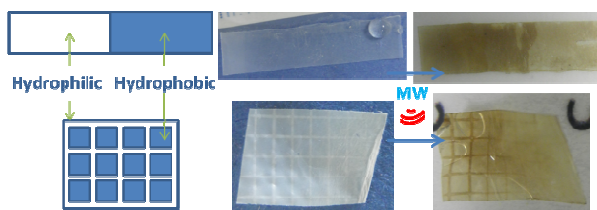


Fig. 9 First column: Scheme of hydrophobic (blue) and hydrophilic (white) patterns in a BC-RD film. Second column: BC-RD films with patterned hydrophobic/hydrophilic zones. A water droplet with large contact angle in the hydrophobic region. Third column: The magnetic nanocomposites. Darker areas with higher iron oxide load correspond to the hydrophilic zones of the patterned cellulose.

Conclusions

Cellulose nanofibers nanocomposited with magnetic NPs have found uses in new applications such as in loudspeakers.¹⁴ Here, we presented a microwave-assisted thermal decomposition method for nanocomposing bacterial cellulose films with superparamagnetic maghemite NPs within only 5 min and without the need for post-synthetic treatment. The NPs are crystalline, less than 10 nm in size, with a narrow particle size distribution. The NPs coat the cellulose films conformally and uniformly, even when the films are folded into complex shapes, and they do not leach when immersed in water for a long time (up to three months). Control over the magnetic fraction was achieved either by employing never-dried cellulose, cellulose films dried by different methods, or by adjusting the initial iron concentration. All films react easily to an external magnetic field, present superparamagnetic behavior at room temperature, and are flexible enough to be bent, even those with the largest magnetic fraction (up to 40 %). Interestingly, the films with the lowest magnetic fraction are also transparent. Finally, we showed preliminary results in a strategy to selectively pattern the bacterial cellulose films with iron oxide NPs. This approach is based on the prior hydrophobization of selected zones of the films. We believe that the approach can be extended to other types of NPs. Moreover, it could allow multiple patterning with several materials. We could, for instance, envisage the drawing of circuits with conductive gold NPs for biodegradable conductive and magnetic implants.

Acknowledgements

This research was funded by the People Program of the European Commission (grant agreement n° 303630, cofounded by the European Social Fund) and the Spanish Ministry of Economy (MAT2012-35324, Consolide-Nanoselect CSD2007-00041). Authors also acknowledge support from COST Action MP1202, the Ramon y Cajal grant RYC-2010-06082 (AL) and the Chinese Scholarship Council fellowship (MZ). PL and WF thank the Helmholtz Association's Initiative and Networking Fund (Grant VH-NG-621) for the support.

Notes and references

- ^a Institut de Ciència de Materials de Barcelona (ICMAB-CSIC), Campus UAB, Bellaterra, Catalonia, E-08193 Spain (alaromaine@icmab.es, roig@icmab.es)
- ^b Karlsruhe Institute of Technology (KIT), Postfach 3640, Karlsruhe, D-76021 Germany

Note: Some of the contents of this manuscript are patent pending

- [†] Electronic Supplementary Information (ESI) available: videos of the materials responding to an external magnetic field, thermogravimetric curves, indexed electron diffraction patterns, magnetic cellulose films immersed in water and table containing materials' characteristics. See DOI:10.1039/b000000x/

1. E. J. Vandamme, S. De Baets, A. Vanbaelen, K. Joris and P. D. Wulf, *Polymer Degradation and Stability*, 1998, **59**, 93-99.
2. A. Svensson, E. Nicklasson, T. Harrah, B. Panilaitis, D. L. Kaplan, M. Britberg and P. Gatenholm, *Biomaterials*, 2005, **26**, 419-431.
3. W. Czaja, A. Krystynowicz, S. Bielecki and R. M. B. Jr., *Biomaterials*, 2006, **27**, 145-151.
4. J. A. Marins, B. G. Soares, H. S. Barud and S. J. Ribeiro, *Mater Sci Eng C Mater Biol Appl*, 2013, **33**, 3994-4001.
5. M. Sureshkumar, D. Y. Siswanto and C.-K. Lee, *Journal of Materials Chemistry*, 2010, **20**, 6948.
6. W. Hu, S. Chen, J. Yang, Z. Li and H. Wang, *Carbohydr Polym*, 2014, **101**, 1043-1060.
7. N. Shah, M. Ul-Islam, W. A. Khattak and J. K. Park, *Carbohydr Polym*, 2013, **98**, 1585-1598.
8. S. Vitta and V. Thiruvengadam, *CURRENT SCIENCE*, 2012, **102**, 1398-1405.
9. D. Breitwieser, M. M. Moghaddam, S. Spirk, M. Baghbanzadeh, T. Pivec, H. Fasl, V. Ribitsch and C. O. Kappe, *Carbohydr Polym*, 2013, **94**, 677-686.
10. J. Wu, Y. Zheng, W. Song, J. Luan, X. Wen, Z. Wu, X. Chen, Q. Wang and S. Guo, *Carbohydr Polym*, 2013.
11. R. T. Olsson, M. A. S. Azizi Samir, G. Salazar-Alvarez, L. Belova, V. Ström, L. A. Berglund, O. Ikkala, J. Nogués and U. W. Gedde, *Nat. Nanotechnol.*, 2010, **5**, 584-588.
12. M. Vural, B. Crowgey, L. C. Kempel and P. Kofinas, *Journal of Materials Chemistry C*, 2014, **2**, 756-763.
13. E. Hendrick, M. Frey, E. Herz and U. Wiesner, *Journal of Engineered Fabrics & Fibers (JEFF)*, 2010, **5**.
14. S. Galland, R. L. Andersson, M. Salajková, V. Ström, R. T. Olsson and L. A. Berglund, *Journal of Materials Chemistry C*, 2013, **1**, 7963-7972.
15. S. Behrens, *Nanoscale*, 2011, **3**, 877-892.
16. Q. Dai and A. Nelson, *Chem Soc Rev*, 2010, **39**, 4057-4066.
17. H. Zhu, S. Jia, T. Wan, Y. Jia, H. Yang, J. Li, L. Yan and C. Zhong, *Carbohydr Polym*, 2011, **86**, 1558-1564.
18. A. Fu, R. J. Wilson, B. R. Smith, J. Mullenix, C. Earhart, D. Akin, S. Guccione, S. X. Wang and S. S. Gambhir, *ACS Nano*, 2012, **6**, 6862-6869.
19. A. Stoica-Guzun, M. Stroescu, S. I. Jinga, I. M. Jipa and T. Dobre, *Industrial Crops and Products*, 2013, **50**, 414-422.
20. S.-M. Li, N. Jia, M.-G. Ma, Z. Zhang, Q.-H. Liu and R.-C. Sun, *Carbohydr Polym*, 2011, **86**, 441-447.
21. A. R. Silva and G. Unali, *Nanotechnology*, 2011, **22**, 315605.
22. M. Baghbanzadeh, L. Carbone, P. D. Cozzoli and C. O. Kappe, *Angew. Chem. Int. Ed.*, 2011, **50**, 11312-11359.
23. Idalia Bilecka, Pierre Elser and M. Niederberger, *ACS Nano*, 2009, **3**, 467-477.
24. D. Monti, A. Ponrouch, M. Estruga, M. R. Palacín, J. A. Ayllón and A. Roig, *Journal of Materials Research*, 2012, **28**, 340-347.
25. O. Pascu, E. Carenza, M. Gich, S. Estradé, F. Peiró, G. Herranz and A. Roig, *The Journal of Physical Chemistry C*, 2012, **116**, 15108-15116.
26. O. Pascu, M. Gich, G. Herranz and A. Roig, *European Journal of Inorganic Chemistry*, 2012, **2012**, 2656-2660.

27. O. Pascu, J. M. Caicedo, M. Lopez-Garcia, V. Canalejas, A. Blanco, C. Lopez, J. Arbiol, J. Fontcuberta, A. Roig and G. Herranz, *Nanoscale*, 2011, **3**, 4811-4816.
28. H. Jin, M. Kettunen, A. Laiho, H. Pynnonen, J. Paltakari, A. Marmur, O. Ikkala and R. H. Ras, *Langmuir*, 2011, **27**, 1930-1934.
29. Y. Habibi, *Chem Soc Rev*, 2014, **43**, 1519-1542.
30. D. Fragouli, I. S. Bayer, R. Di Corato, R. Brescia, G. Berton, C. Innocenti, D. Gatteschi, T. Pellegrino, R. Cingolani and A. Athanassiou, *Journal of Materials Chemistry*, 2012, **22**, 1662-1666.
31. M. Zeng, A. Laromaine and A. Roig, *Submitted*, 2014.
32. M. Niederberger and G. Garnweitner, *Chemistry*, 2006, **12**, 7282-7302.
33. S. Kalhori, B. Minaev, S. Stone-Elander and A. N. Elander, *J. Phys. Chem. A*, 2002, **106**, 8516-8524.

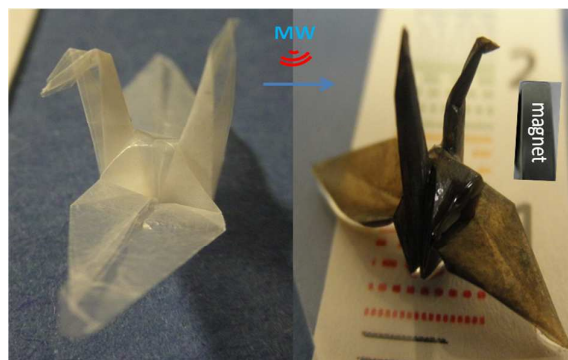
Origami magnetic cellulose: controlled magnetic fraction and patterning of flexible bacterial cellulose

Muling Zeng¹, Anna Laromaine^{1*}, Wenqian Feng², Pavel A. Levkin², Anna Roig^{1*}

¹ Institut de Ciència de Materials de Barcelona (ICMAB-CSIC), Campus UAB, Bellaterra, Catalonia, E-08193 Spain (alaromaine@icmab.es, roig@icmab.es)

² Karlsruhe Institute of Technology (KIT), Postfach 3640, Karlsruhe, D-76021 Germany

TOC



Superparamagnetic, flexible and transparent bacterial cellulose films by very fast microwave-assisted synthesis with control over the magnetic fraction and magnetic patterning

KEYWORDS: Bacterial cellulose, microwave synthesis, nanocomposites, superparamagnetic iron oxide.